

# Journal of Biomedical Optics

[SPIEDigitalLibrary.org/jbo](http://SPIEDigitalLibrary.org/jbo)

## **Carcinogenic damage to deoxyribonucleic acid is induced by near-infrared laser pulses in multiphoton microscopy via combination of two- and three-photon absorption**

Oleg Nadiarnykh  
Giju Thomas  
Johan Van Voskuilen  
Henricus J. C. M. Sterenborg  
Hans C. Gerritsen

# Carcinogenic damage to deoxyribonucleic acid is induced by near-infrared laser pulses in multiphoton microscopy via combination of two- and three-photon absorption

Oleg Nadiarnykh,<sup>a</sup> Giju Thomas,<sup>b</sup> Johan Van Voskuilen,<sup>a</sup> Henricus J. C. M. Sterenborg,<sup>b</sup> and Hans C. Gerritsen<sup>a</sup>

<sup>a</sup>Utrecht University, Debye Institute, Molecular Biophysics, Princetonplein 5, 3508 TA Utrecht, The Netherlands

<sup>b</sup>Erasmus Medical Center, Center for Optical Diagnostics and Therapy, POB 2040, NL-3000 CA Rotterdam, The Netherlands

**Abstract.** Nonlinear optical imaging modalities (multiphoton excited fluorescence, second and third harmonic generation) applied *in vivo* are increasingly promising for clinical diagnostics and the monitoring of cancer and other disorders, as they can probe tissue with high diffraction-limited resolution at near-infrared (IR) wavelengths. However, high peak intensity of femtosecond laser pulses required for two-photon processes causes formation of cyclobutane-pyrimidine-dimers (CPDs) in cellular deoxyribonucleic acid (DNA) similar to damage from exposure to solar ultraviolet (UV) light. Inaccurate repair of subsequent mutations increases the risk of carcinogenesis. In this study, we investigate CPD damage that results in Chinese hamster ovary cells *in vitro* from imaging them with two-photon excited autofluorescence. The CPD levels are quantified by immunofluorescent staining. We further evaluate the extent of CPD damage with respect to varied wavelength, pulse width at focal plane, and pixel dwell time as compared with more pronounced damage from UV sources. While CPD damage has been expected to result from three-photon absorption, our results reveal that CPDs are induced by competing two- and three-photon absorption processes, where the former accesses UVA absorption band. This finding is independently confirmed by nonlinear dependencies of damage on laser power, wavelength, and pulse width. © 2012 Society of Photo-Optical Instrumentation Engineers (SPIE). [DOI: 10.1117/1.JBO.17.11.116024]

Keywords: autofluorescence; carcinogenic damage; diagnostic *in vivo* imaging; imaging multiphoton microscopy.

Paper 12527 received Aug. 15, 2012; revised manuscript received Oct. 23, 2012; accepted for publication Oct. 25, 2012; published online Nov. 19, 2012.

## 1 Introduction

In recent years, nonlinear optical imaging (NLO) modalities based on near-infrared (NIR, 700 to 1000 nm) femtosecond-laser sources have been increasingly utilized in biomedical research and clinical applications. *In vivo* tissue imaging is especially promising for investigation, diagnostics, and monitoring of cancers and other disorders. Multiphoton laser scanning microscopy (multiphoton excited fluorescence, second and third harmonic generation) can probe tissue structure at high diffraction-limited resolution (0.3  $\mu\text{m}$ ), with 100- to 300- $\mu\text{m}$  penetration depth, intrinsic three-dimensionality (3-D), and no out-of-focal volume photobleaching/photodamage, since there are no one-photon absorbers except melanin at NIR wavelengths.

Cells and tissues contain a host of endogenous fluorophores that can be excited using multiphoton imaging techniques. Contrast in tissue arises from autofluorescence of, among others, nicotinamide adenine dinucleotide (NADH, absorption maximum at 340 nm),<sup>1</sup> flavin adenine nucleotide (FAD, 440 nm),<sup>1</sup> melanin (broad-band absorption through all visible wavelengths),<sup>2</sup> collagen (Type I, 375 nm),<sup>3</sup> and various lipoproteins, while noncentrosymmetric protein arrays (collagen, myosin and tubulin) produce a second harmonic signal,<sup>4</sup> and interfaces can be visualized with third harmonic generation.<sup>5,6</sup> All these distinct endogenous sources can be excited simultaneously and discriminated in a spectral imaging system.<sup>7-9</sup> NLO spectral

imaging based on label-free autofluorescence has been demonstrated *in vivo* not only in skin,<sup>10</sup> but also in highly dynamic tissues such as lymphoid tissue<sup>11</sup> and intestine.<sup>12</sup> Moreover, *in vivo* monitoring of protein-bound and free NADH has been achieved recently with NLO spectral imaging.<sup>13</sup>

Thus NLO imaging allows for probing and understanding of cells and tissues in their natural unperturbed state. The ability to generate images using intrinsic sources opens new possibilities for development of NLO imaging in medical applications in hospital settings, where label-based imaging must be avoided.

To this date, NLO imaging has been shown to successfully visualize and distinguish with statistical significance between control and diseased states in various tissue disorders,<sup>14-22</sup> as well as detect and monitor changes in free and bound NAD (P)H in cancer versus normal cells,<sup>23</sup> and during apoptosis.<sup>13</sup>

Apart from technical challenges for *in vivo* microscopy, one of the reasons for a delay in routine NLO imaging in clinical applications is insufficient experimental data on possible risks involved, with carcinogenic cell damage being the most serious concern.<sup>24,25</sup> For a successful transition from laboratory bench to clinics, biological safety must be investigated thoroughly.

Since all multiphoton processes are based on simultaneous nonresonant absorption or resonant up-conversion of two or three excitation photons in the sub-femtoliter focal volume of a high-NA objective, they require femtosecond laser pulses with high peak intensity in the range of several hundreds of  $\text{GW}/\text{cm}^2$ . This level of photon density is high enough to cause destructive nonlinear photochemical effects in live

Address all correspondence to: Oleg Nadiarnykh, University, Debye Institute, Molecular Biophysics, Princetonplein 5, 3508 TA Utrecht, The Netherlands. Tel: +31 30 2532344; Fax: +31 30 253 2706; E-mail: o.nadyarnykh1@uu.nl

cells, with acute damage ranging from irreversible impairment of cell division,<sup>26</sup> formation of destructive oxygen radicals and singlet oxygen<sup>27</sup> to plasma formation and morphological destruction, where the latter require an order of magnitude higher intensity.<sup>28</sup> In fact, thermal damage resulting from multi-photon water absorption has been estimated to be insignificant throughout the near-infrared imaging range on the order of 1 mK for typical excitation power of 5 to 30 mW.<sup>29</sup>

However, the biggest safety concern has always been the direct DNA damage from simultaneous absorption of three photons, as strong absorption bands of nucleic acids lie below 290 nm, peaking at 257 nm. The DNA lesions induced are similar to those from natural UV exposure resulting in formation of cyclobutane-pyrimidine dimers (CPDs), 6-4 photo-products, single- and double-strand breaks, and numerous modified bases.<sup>25,30-32</sup> Among all these lesions, CPDs are primarily responsible for carcinogenesis<sup>33</sup> resulting from a series of mutations in cells with unrepaired damage.<sup>34</sup> The genotoxic cellular effects of the shorter UV wavelengths (UVC band, 200 to 290 nm, and UVB band, 290 to 320 nm) have been long known and thoroughly investigated.<sup>30,35-37</sup> However, the DNA damaging effects of longer wavelengths (UVA band, 320 to 400 nm) causing strong mutagenic properties have been recognized only recently.<sup>30,38-40</sup> There is an ongoing debate regarding the direct and indirect pathways leading from UVA absorption to CPDs. Several studies have claimed that UVA absorption produces reactive chemical species that can damage DNA.<sup>14,38-42</sup> However, two recent studies strongly suggested that CPDs are produced by UVA via direct photochemical mechanism, without mediation of a cellular photosensitizer or intermediate reactive species.<sup>43,44</sup> Moreover, Mouret et al. showed evidence that UVA-induced CPDs are less repairable.<sup>38</sup> In their experiment, 48 h after exposure to UVA radiation the level of unrepaired CPDs was unexpectedly higher than after UVB-induced damage. There are no indications that different CPD dimers are produced by absorption of UVA and UVC photons. However, the possible explanations for persistence of UVA-induced CPDs include different in-cell cycle arrest after irradiation, degradation of DNA repair protein by the UVA-induced reactive oxygen species<sup>37</sup> as well as alteration of cell behavior through changes in cell signaling pathways by UVA radiation.<sup>45</sup>

Theoretically, in the spectral range typically used for NLO imaging of endogenous fluorophores both UVC and UVA absorption bands can be excited by femtosecond laser pulses via three- and two-photon absorption, respectively. Previously, only third-order process and UVC-like damage has been considered.<sup>25</sup> Therefore we saw the need to investigate the mechanism of CPD damage by near-IR laser pulses. Specifically it is important to understand if CPD damage results from concurrent three- and two-photon absorption, and if it does what their contributions are.

## 2 Materials and Methods

### 2.1 Cell Culture

Chinese hamster ovary (CHO) cells were cultured in flasks containing Dulbecco's modified Eagle's medium (Invitrogen, Breda, The Netherlands) containing 7.5% fetal calf serum (Invitrogen), 2 mM L-glutamine (Invitrogen), and 2% antibiotic mix (Invitrogen) at pH 7.4. Cultures were maintained at 37°C in an incubator aerated with 5% CO<sub>2</sub>.

For experiments, cells were trypsinized and 3 ml of the cell suspension was transferred into sterile petri dishes of 35 mm diameter with an inbuilt glass cover slip of 0.16 to 0.19 mm thickness and 20 mm diameter (MatTek, USA), located in the petri dish center for optimal laser irradiation/imaging. Grids were drawn on the petri dish bottom in order to image known groups of cells with varying laser parameters. To obtain a confluent monolayer of cells the cell chambers were additionally incubated for another day under the above conditions.

### 2.2 Laser Irradiation

The cells were imaged with a laser scanning unit (C1, Nikon, Japan) mounted on an inverted microscope (TE2000, Nikon, Japan) coupled to a mode-locked titanium sapphire femtosecond laser (Chameleon model, Coherent, USA) with 80-MHz pulse repetition rate, and 130-fs pulse width. Excitation intensity was controlled with a combination of a half-waveplate and a polarizing cube (Thorlabs, USA). Pulse width was adjusted with a group velocity dispersion compensator consisting of a pair of gratings (Thorlabs, USA) and measured at the focal plane with an autocorellator (APE GmbH, Germany). All experiments were performed over a range of excitation wavelengths between 695 and 810 nm with varied intensity and pulse width using a water immersion 40×0.8 N.A. objective (Nikon, Japan) with autofluorescence signal acquired in a nondescanned configuration.

Confluent monolayers of CHO cells were exposed to NIR irradiation doses under varying imaging conditions. The acquired xyz optical stacks contained between 10 and 12 images of 512×512 pixel (170×170 μm) size with axial intervals of 1 μm. The cells in the nonirradiated regions served as an internal negative control. UV-irradiation was performed in a UV cabinet (Chromato Vue CC-20, USA) over the whole surface of the petri dishes at two individual wavelengths: 254 nm corresponding to UVC band, and 365 nm corresponding to UVA band.

### 2.3 Immuno-Fluorescence Assay for CPDs

After the NIR irradiation the cells were fixed for 10 min with 4% formalin (Sigma Aldrich) in phosphate buffered saline (PBS). Washing the cells with 2 mL PBS five times followed this step and every subsequent one. Fixed cells were incubated for 5 min on ice with 0.5% Triton X-100 in PBS in order to permeabilize the cell membranes for antibody penetration. The cellular DNA was then denatured by treating the samples with 2N HCL at room temperature for 30 min. Primary monoclonal antibodies specific for CPDs (Cosmobio, Japan) were diluted 1:500 in 5% bovine serum albumin in PBS and incubated with the cells for 1 h at room temperature. For the secondary antibodies, we used goat anti-mouse IgG conjugated with AlexaFluor-594 (Invitrogen, Germany) diluted 1:100 in 5% bovine serum albumin in PBS, where incubation was performed for 30 min at room temperature. Finally, the cells were stained with 0.05 μg/mL DAPI in PBS to facilitate visual localization of nuclei during the analysis. The samples were dried and mounted with Vectashield antifade medium, and the petri dishes were closed and sealed with paraffin tape.

The one-photon CPD immuno-fluorescence from the stained cells was recorded using an EMCCD camera (Cascade model, Photometrics, USA) coupled to a fluorescence microscope (TE2000, Nikon, Japan) with a 20×0.75 NA PlanApo air objective (Nikon, Japan). Since formalin fixation is known to

flatten cells, acquisition of a single optical section from the axial center of cells is a sufficient indicator of the total fluorescence. Signal intensity was quantified using ImageJ software (<http://rsbweb.nih.gov/ij/>), where pixel intensity values were obtained from individual nuclei, and then averaged between all the cells irradiated under the same conditions. All samples were imaged using the same acquisition parameters with minimal and similar levels of photobleaching. Therefore the quantified fluorescence intensity serves as a valid metric for the amount of induced CPD lesions. Every set of simultaneously processed samples had one UVC-irradiated sample that served as positive control and provided a normalization factor for comparison between different sets to account for unavoidable fluctuations in staining efficiency and inhomogeneity.

### 3 Results and Discussion

A typical image of two-photon excited autofluorescence from cells is shown in Fig. 1(a) along with the corresponding one-photon immuno-fluorescence from CPDs in the nuclei of fixed cells [Fig. 1(b)]. We note a very minimal cell migration between the start of irradiation and fixation with formalin. A clear border of region with CPD damage corresponds to the edge of the  $x$ - $y$  scan; the cells in the area unexposed to laser exhibit a very low level of CPD immuno-fluorescence. We attribute the background level of CPDs in the cells to CPDs formed by exposure to stray white light during culturing and especially during the experiment. Nonspecificity of the CPD staining was ruled out by a separate negative control experiment. Therefore any quantification of the laser-induced damage accounted for the fluorescence value from the cells unexposed to laser. As expected, CPD damage from imaging with femtosecond laser is evenly distributed within cell nuclei as equal doses of radiation are delivered to every pixel. Any inhomogeneity in the damage pattern corresponds to local concentration of available DNA. On the contrary, CPDs induced by UVC lamp [positive control, Fig. 1(c)] show a doughnut-shape distribution with stronger damage at the nuclei periphery. This finding can be explained by strong absorption of 254-nm photons by DNA. It has been shown<sup>32</sup> that in some laser-damaged cells lesions tend to migrate toward the periphery of the nuclei, suggesting that peripheral damage might be preferred by cellular repair mechanisms. Therefore the possibility that uniformly damaged nuclei might carry different consequences for cell viability, repair, and carcinogenic mutations requires further investigation.

#### 3.1 Intensity Versus Damage

Experimentally measured dependence of CPD damage on peak intensity for three different wavelengths at fixed pulse width of 175 fs (measured at the sample) is plotted in Fig. 2. We note there is apparent minimal peak intensity around  $0.35 \text{ TW/cm}^2$  that produces detectable damage just above the background level. However, this is indicative of the overall staining method sensitivity at lower levels of CPDs rather than a threshold behavior. Nevertheless, these laser intensities are lower than required for tissue imaging ( $0.5$  to  $0.8 \text{ TW/cm}^2$ ), and the damage over this practical range of intensities is investigated here. As evident from the data, the minimal peak intensity that produces detectable damage decreases, while the level of CPD damage increases for shorter wavelengths.

Any third-order process would be governed by cubic power dependence. While accounting for the background level (parameter  $A_0$ , Table 1) of CPD immuno-fluorescence from

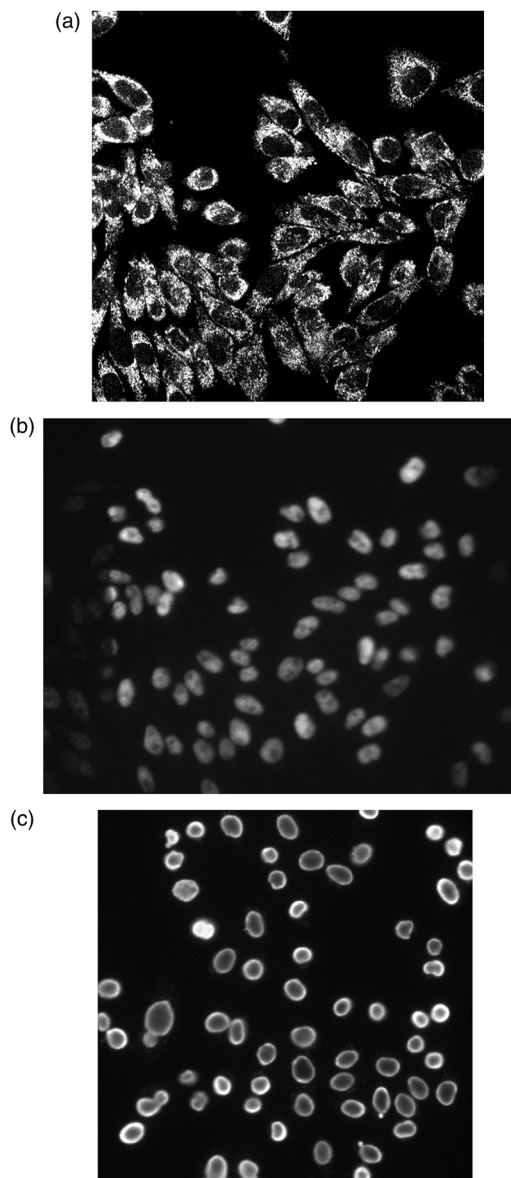


**Fig. 1** Experimental recording of CPD damage: (a) two-photon excited autofluorescence from cells imaged at 730 nm; (b) corresponding immunofluorescence image of cell nuclei with CPD damage (note on the left side the distinct border of the laser scanned with residual level of fluorescence signal); (c) CPD immunofluorescence from cell nuclei irradiated with UVC light (note the mostly peripheral distribution of CPD lesions).

nonirradiated cells, linear fits of the experimental data on the log-log scale yielded slopes of  $3.40 \pm 0.33$ ,  $2.94 \pm 0.18$ , and  $2.81 \pm 0.16$  for 780, 750, and 711 nm, respectively. Clearly, these results show within the experimental error a three-photon nature of CPD damage at longer wavelengths. However, the decline in slope value of power dependence with shorter wavelengths points to the apparent sub-third-order behavior at 711 nm. In fact, if shorter wavelengths give rise to two-photon absorption corresponding to UVA absorption band, the total CPD damage would result from a superposition of the second and the third-order events.

In order to independently verify our finding that CPD lesions are induced by simultaneous combination of two- and three-photon absorption below 780 nm we investigated dependence

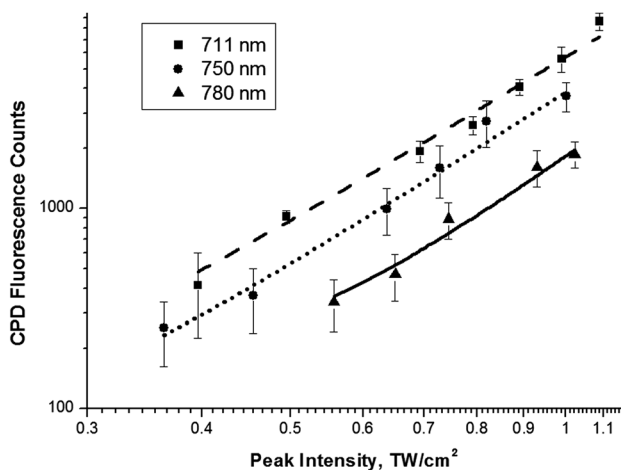


**Fig. 2** Logarithmic plot of CPD immunofluorescence signal dependence on peak intensity of laser. The slopes of the linear fits are  $3.40 \pm 0.33$ ,  $2.94 \pm 0.18$ , and  $2.81 \pm 0.16$  for 780, 750, and 711 nm, respectively. Scan speed:  $30 \mu\text{s}$ , pulsewidth at the focal plane: 164 fs.

of CPD damage on pulse width of excitation laser at the wavelength of 750 nm and constant intensity.

For  $n$ -photon absorption process, the number of photons absorbed per molecule ( $n_a$ ) is given by<sup>46</sup>

$$n_a \approx \frac{P_0^n \sigma_{n-ph}}{f_{\text{rep}}^{(n-1)} \tau^{(n-1)}} \left( \frac{NA^2}{2hc\lambda} \right)^n, \quad (1)$$

where  $n$  equals 2 and 3 for 2- and 3-photon absorption, respectively,  $P$  is the average excitation power,  $\sigma_{n-ph}$  is the multiphoton absorption cross-section (in context of this discussion corresponds to CPD-inducing transitions),  $f_{\text{rep}}$  is laser repetition rate,  $\tau$  is the excitation pulse width,  $\lambda$  is the excitation wavelength,  $c$  is the speed of light,  $h$  is Planck's constant. We note here, that two-photon absorption is inversely proportional to the excitation pulse width, while three-photon absorption scales down proportionally to the square of the pulse width. However, for coexisting multiphoton processes one would expect an intermediate coupled behavior.

The pulse widths used for imaging are normally above 100 fs, as shorter pulses get severely broadened by the microscope optics through group velocity dispersion. In our experiment, CPD damage was recorded at 750 nm with constant intensity of 14 mW while varying pulse width at the focal plane from 164 to 425 fs with a grating pair, and the results are plotted in Fig. 3. While the intensity of 14 mW is on the high end of the levels expected for cell imaging, it provided

**Table 1** Results of fitting the experimental data of CPD damage dependence on peak intensity.

Wavelength	$A_0$	$A_2$	$A_3$	R-squared value
711 nm	63	$886 \pm 655$	$4772 \pm 927$	0.9717
750 nm	40	$126 \pm 433$	$3663 \pm 624$	0.9769
780 nm	130	$0 \pm 470$	$1599 \pm 589$	0.9422

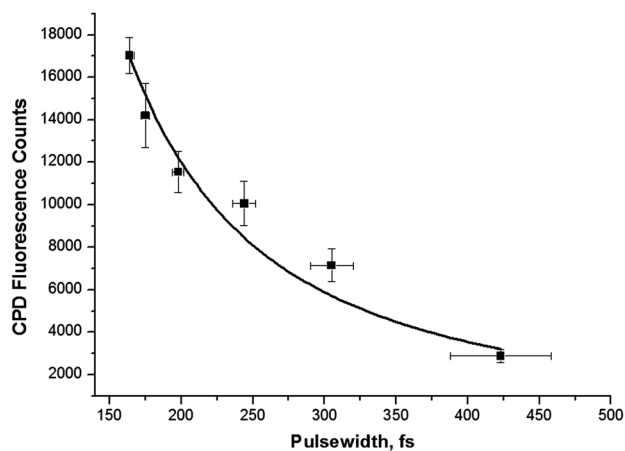


**Fig. 3** Pulsewidth dependence of CPD damage recorded at 750 nm with 14 mW average intensity and  $30 \mu\text{s}$  pixel dwell time.

the necessary dynamic range for excitation with 425-fs pulse width. As described above, several spots in the same cell dish were imaged with different pulse widths in order to have the same staining conditions within the data series. Using, Eq. (1), the fit of the experimental data yielded the exponential value ( $n^{-1}$ ) of  $1.76 \pm 0.18$  confirming our previous finding that damage arises from a mixture of two- and three-photon absorption. This dependence suggests that at longer pulse widths contribution from two-photon absorption increases as reduced photon density makes three-photon absorption less efficient. Indeed, a rapid decrease of induced CPD damage is evident between 164 and 200 fs, while this trend slows down as excitation pulse is broadened further.

Earlier, König et al. reported the evidence of a strong effect of excitation pulse width at 780 nm on CPD damage.<sup>47</sup> However, the damage was shown as purely two-photon following the ( $P^2/\tau$ ) relation. The discrepancy with our finding is likely due to the different methods of damage assessment. While our data accounts for total induced CPD damage based on immediate immunofluorescent assay, König et al. estimated residual damage by monitoring cell-cloning efficiency for 48 h after the exposure to laser. The latter approach obviously includes not only the direct damage, but also the subsequent cellular response (repair and apoptosis). Therefore it cannot be indicative of the actual order of absorption and the physics involved. On the other hand, if we consider the two findings together, second- and third-order dependence of direct CPD damage and second-order dependence of cloning efficiency on laser intensity at 780 nm, one can speculate that stronger initial damage has sub-linear effect on cell viability.

The pulse width dependence investigated here has implications for *in vivo* imaging with ultrashort pulses, such as two-photon microscopy with pulse widths as low as 12 femtoseconds.<sup>48</sup> On one hand, decreasing the pulse width translates into linear increase of two-photon excited fluorescence intensity. At the same time, as we demonstrated here, the CPD damage increases as  $\tau^{1.76}$  (on average), and proportionally to the subcubic peak intensity under the typically used imaging conditions. For much shorter pulses, the damage will be caused by almost 100% third-order absorption overshadowing the gain in fluorescence efficiency. The increased damage can only be offset by the corresponding decrease in the average excitation intensity in order to maintain the same peak intensity of the pulses.

However, this damage cannot be compensated for without loss of intensity and, consequently, image quality.

Having demonstrated the superposition of competing two- and three-photon processes, we can decouple their relative contributions by refitting the data from Fig. 2 with the following equation:

$$\text{CPD} \sim A_0 + A_2 I^2 + A_3 I^3, \quad (2)$$

where  $A_0$  is the background CPD level in nonexposed cells,  $I$  is the damaging intensity, while  $A_2$  and  $A_3$  are the fitting parameters. The results are plotted in Fig. 4 and listed in Table 1. The R-squared values are not significantly different from those of the earlier fits plotted in Fig. 2, and fall between 0.942 and 0.977. However, now this simple model shows relative contributions of two- and three-photon absorption (UVA- and UVC-like CPD damage, respectively), where the latter dominates at all wavelengths investigated, even at 711 nm. Moreover, the fits estimate how this distribution changes with increasing intensity, eventually becoming almost exclusively third order. The data shows that at 711 nm, the share of two-photon process falls from 38% to 16% as peak intensity increases from 0.3 to 1 TW/cm<sup>2</sup>. The data shows a weak but nonnegligible contribution of second order absorption at 750 nm (falling from 10% to 3% over the same intensity range), and pure three-photon absorption at 780 nm. In fact, the 780 nm data series exhibits better conversion when fitted with only third-order term. We note that adding the fourth-order term to the model does not improve the fitting statistics thus diffusing any concerns about possible CPD-producing absorption below 200 nm.

### 3.2 Wavelength Dependence

To further investigate the relative contributions of two- and three-photon absorption, we looked at spectral response of CPD damage. A strong dependence of induced CPD damage on excitation wavelength was found, as can be seen on Fig. 5. For this experiment, only the wavelength was varied, while intensity and pulse width were maintained constant. Although the damage level is low for wavelengths above 780 nm, where the absorption is purely three-photon according to the intensity dependence discussed above, a moderate

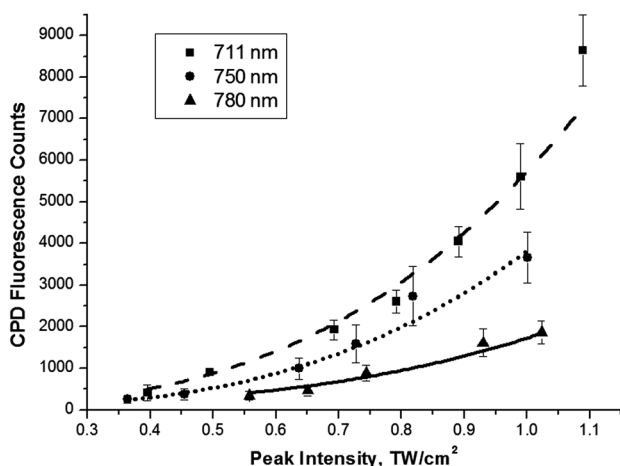


**Fig. 4** CPD immunofluorescence signal dependence on peak intensity of laser. The fits to Eq. (2)  $\text{CPD} \sim A_0 + A_2 I^2 + A_3 I^3$  are used to decouple the relative contributions of two- and three-photon absorption to CPD damage. Pixel dwell time: 30  $\mu\text{s}$ , pulsewidth at the focal plane: 164 fs.

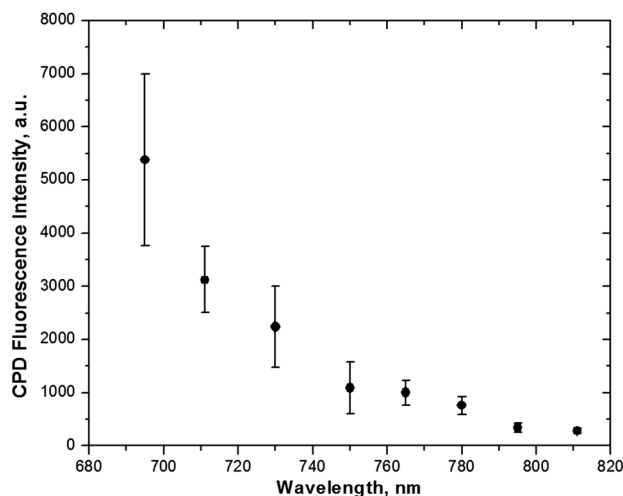


**Fig. 5** Spectral dependence of CPD damage production. Pixel dwell time: 30  $\mu\text{s}$ , pulsewidth at the focal plane: 164 fs.

increase in damage with shorter wavelengths is observed for the 780- to 750-nm range, followed by a dramatic threefold rise of CDP formation over 750- to 710-nm range. The factors that must be considered for the explanation of this trend act oppositely. On one hand, one-photon DNA absorption is considerably stronger at UVC range (peaking between 255 and 260 nm) than at UVA. This translates into the eightfold higher CPD damage produced by UVC lamp as compared with that from UVA lamp in our positive control experiment. On the other hand, compared with three-photon absorption, two-photon process has at least an order of magnitude higher probability and occurs over a larger focal volume. At longer wavelengths, the absorption bands of endogenous cellular fluorophores are excited primarily. However, as the excitation wavelength becomes short enough (<750 nm) to access the low UVA band, the two-photon absorption quickly becomes an important and efficient mechanism of CPD damage, although still much weaker than the three-photon effect.

We note the excessive CPD damage at 695 nm, where the data has the largest error bars. In fact, we have experienced problems with keeping cells still attached to the cell dish between exposure at 695 nm and fixation with formaldehyde. The cell loss was so high that measurement of excitation power dependence at this wavelength was not feasible, as it requires successive irradiation of several spots with 695-nm wavelength. Here the laser easily excites UVA and UVC absorption bands with high efficiency. We speculate that cumulative absorption at 695 nm is so strong that cell necrosis and/or apoptosis mechanisms are triggered immediately. Fortunately, for *in vivo* imaging, all endogenous fluorophores can still be excited above 750 nm, so the extreme levels of CPD damage observed at shorter wavelengths do not present additional practical concerns.

Our results suggest that imaging with wavelengths above 1000 nm would dramatically, if not completely, reduce the CPD carcinogenic risk since only the long-wavelength edge of UVA absorption band might be excited with three-photon absorption.

### 3.3 Effect of Radiation Dose

A linear dependence of CPD damage on scan speed is observed in our experiments, where we maintained constant peak

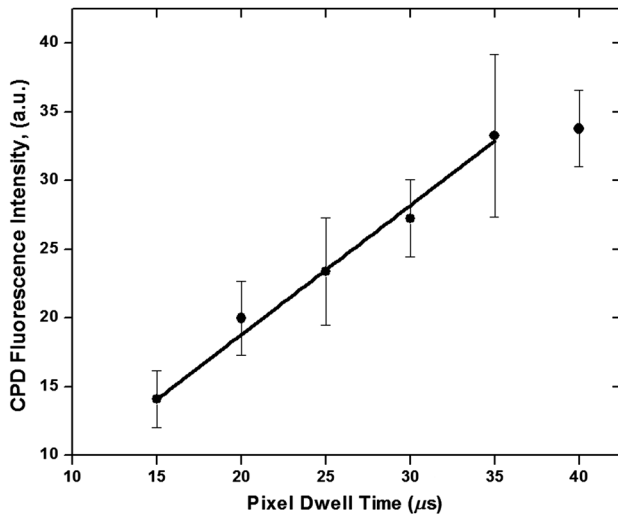


Fig. 6 Linear effect of pixel dwell time on induction of CPD lesions, pulsewidth at the focal plane: 164 fs.

intensity at 750 nm (Fig. 6). As expected, pixel dwell time is directly proportional to the number of multiphoton absorption events in DNA. We note the apparent damage saturation at exposure time of 40  $\mu$ s. This could be due to complete DNA dimerization and/or acute effects that cause cells detachment and loss prior to fixation and staining.

### 3.4 Considerations for Tissue Imaging

The main finding of this study was that the CPD damage is induced by a combination of two- and three-photon absorption processes, where the relative contributions are dependent on imaging parameters. Our conclusions are made based on DNA absorption properties within one-pixel resolution. When translating these findings into the highly scattering environment of biological tissues, attenuation of excitation as well as defocussing must be considered. The attenuation will reduce average excitation intensity, while defocussing will further decrease the peak excitation intensity at the focal volume. Additionally, the relative volumes that are subject to significant two- and three-photon fluorescence (based on  $1/e^2$  intensity profile) will change. However, as can be estimated<sup>49</sup> with focused Gaussian beam approximation, the volume changes alone does not significantly alter the total CPD production over 200  $\mu$ m depth in human skin. Finally, we expect the scattering effectively affects these imaging parameters resulting in the corresponding combination of two- and three-photon CPD damage within the exposed focal volume.

## 4 Conclusion

This paper demonstrates for the first time to the best of our knowledge that the CPD damage of the cellular DNA induced during imaging with femtosecond near-IR laser results from concurrent two- and three-photon absorption. Effectively, these processes correspond to damage caused by UVA and UVC irradiation, respectively. The third-order absorption is the dominant mechanism, where its contribution increases with wavelength and intensity, while it decreases with pulse width. At all wavelengths required for practical *in vivo* tissue imaging the third-order absorption (UVC-like damage) is responsible for more than 85% of the CPDs induced. However,

as discussed above the mechanisms and implications of the CPD damage caused by absorption in the UVA band are still debated in the literature, as they might be different from those at the UVC band and might include a combination of direct absorption by DNA and damage by intermediate reactive species. Therefore, for a thorough evaluation of any risks involved during *in vivo* two-photon excited fluorescence imaging both mechanisms of CPD formation must be considered separately with decoupled relative contributions, and according to their carcinogenic potential. Finally, post-exposure cellular responses (repair and apoptosis) to CPD lesions with respect to different proportion of UVA- and UVC-like damage warrant further investigation, preferably *in vivo*, where various cell types must be studied.

## References

1. D. W. Piston, B. R. Masters, and W. W. Webb, "Three-dimensionally resolved NAD(P)H cellular metabolic redox imaging of the in situ cornea with two-photon excitation laser scanning microscopy," *J. Microsc.* **178**(1), 20–27 (1995).
2. L. O. Svaasand et al., "Tissue parameters determining the visual appearance of normal skin and port-wine stains," *Lasers Med. Sci.* **10**(1), 55–65 (1995).
3. A. Zoumi, A. Yeh, and B. J. Tromberg, "Imaging cells and extracellular matrix *in vivo* by using second-harmonic generation and two-photon excited fluorescence," *Proc. Natl. Acad. Sci. U.S.A.* **99**(17), 11014–11019 (2002).
4. P. J. Campagnola and L. M. Loew, "Second-harmonic imaging microscopy for visualizing biomolecular arrays in cells, tissues and organisms," *Nat. Biotechnol.* **21**(11), 1356–1360 (2003).
5. C.-K. Sun et al., "Higher harmonic generation microscopy for developmental biology," *J. Struct. Biol.* **147**(1), 19–30 (2004).
6. D. Débarre et al., "Imaging lipid bodies in cells and tissues using third-harmonic generation microscopy," *Nat. Methods* **3**(1), 47–53 (2006).
7. T. Haraguchi et al., "Spectral imaging fluorescence microscopy," *Genes Cells* **7**(9), 881–887 (2002).
8. V. Ulrich et al., "Compact multiphoton/single photon laser scanning microscope for spectral imaging and fluorescence lifetime imaging," *Scanning* **26**(5), 217–225 (2004).
9. J. A. Palero et al., "*In vivo* nonlinear spectral imaging in mouse skin," *Opt. Express* **14**(10), 4395–4402 (2006).
10. J. A. Palero et al., "*In vivo* nonlinear spectral imaging microscopy of visible and ultraviolet irradiated hairless mouse skin tissues," *Photochem. Photobiol. Sci.* **7**(11), 1422–1425 (2008).
11. P. Steven et al., "Experimental induction and three-dimensional two-photon imaging of conjunctiva-associated lymphoid tissue," *Invest. Ophthalmol. Visual Sci.* **49**(4), 1512–1517 (2008).
12. R. Orzekowsky-Schroeder et al., "*In vivo* spectral imaging of different cell types in the small intestine by two-photon excited autofluorescence," *J. Biomed. Opt.* **16**(11), 116025 (2011).
13. J. A. Palero et al., "*In vivo* monitoring of protein-bound and free NADH during ischemia by nonlinear spectral imaging microscopy," *Biomed. Opt. Express* **2**(5), 1030–1039 (2011).
14. R. Cicchi et al., "Multidimensional non-linear laser imaging of basal cell carcinoma," *Opt. Express* **15**(16), 10135–10148 (2007).
15. O. Nadiarykh et al., "Second harmonic generation imaging studies of diseased states," *Microsc. Microanal.* **14**(Suppl. 2), 736–737 (2008).
16. E. Dimitrow et al., "Sensitivity and specificity of multiphoton laser tomography for *in vivo* and *ex vivo* diagnosis of malignant melanoma," *J. Invest. Dermatol.* **129**(7), 1752–1758 (2009).
17. T.-L. Sun et al., "Label-free diagnosis of human hepatocellular carcinoma by multiphoton autofluorescence microscopy," *Appl. Phys. Lett.* **95**(19), 193703 (2009).
18. C.-C. Wang et al., "Differentiation of normal and cancerous lung tissues by multiphoton imaging," *J. Biomed. Opt.* **14**(4), 044035 (2009).
19. K. König et al., "Clinical optical coherence tomography combined with multiphoton tomography of patients with skin diseases," *J. Biophoton.* **2**(6–7), 389–397 (2009).

20. C.-Y. Dong and P. J. Campagnola, "Optical diagnostics of tissue pathology by multiphoton microscopy," *Expert Opinion on Medical Diagnostics* **4**(6), 519–529 (2010).
21. D. K. Bird et al., "Metabolic mapping of MCF10A human breast cells via multiphoton fluorescence lifetime imaging of the coenzyme NADH," *Cancer Res.* **65**(19), 8766–8773 (2005).
22. M. W. Conklin et al., "Fluorescence lifetime imaging of endogenous fluorophores in histopathology sections reveals differences between normal and tumor epithelium in carcinoma in situ of the breast," *Cell Biochem. Biophys.* **53**(3), 145–157 (2009).
23. O. Nadiarykh et al., "Alterations of the extracellular matrix in ovarian cancer studied by Second Harmonic Generation imaging microscopy," *BMC Cancer* **10**(94) (2010).
24. H. J. Sterenborg et al., "Evaluation of skin cancer risk resulting from long term occupational exposure to radiation from ultraviolet lasers in the range from 190 to 400 nm," *Photochem. Photobiol.* **54**(5), 775–780 (1991).
25. R. A. Meldrum and S. W. Botchway, "Nanoscale spatial induction of ultraviolet photoproducts in cellular DNA by three-photon near-infrared absorption," *EMBO Rep.* **4**(12), 1144–1149 (2003).
26. K. König et al., "Cellular response to near-infrared femtosecond laser pulses in two-photon microscopes," *Opt. Lett.* **22**(2), 135–136 (1997).
27. M. L. Cunningham et al., "Photosensitized production of superoxide anion by monochromatic (290–405 nm) ultraviolet irradiation of NADH and NADPH coenzymes," *Photochem. Photobiol.* **42**(2), 125–128 (1985).
28. K. König et al., "Two-photon excited lifetime imaging of autofluorescence in cells during UVA and NIR photostress," *J. Microsc.* **183**(3), 197–204 (1996).
29. A. Schönle and S. W. Hell, "Heating by absorption in the focus of an objective lens," *Opt. Lett.* **23**(5), 325–327 (1998).
30. A. Besaratinia et al., "DNA lesions induced by UVA1 and B radiation in human cells: Comparative analyses in the overall genome and in the p53 tumor suppressor gene," *Proc. Natl. Acad. Sci. U.S.A.* **102**(29), 10058–10063 (2005).
31. J. Cadet, E. Sage, and T. Douki, "Ultraviolet radiation-mediated damage to cellular DNA," *Mutat. Res. Fundament. Molec. Mech. Mutagen.* **571**(1–2), 3–17 (2005).
32. F. Fischer et al., "Risk estimation of skin damage due to ultrashort pulsed, focused near-infrared laser irradiation at 800 nm," *J. Biomed. Opt.* **13**(4), 041320 (2008).
33. L. Marrot and J.-R. Meunier, "Skin DNA photodamage and its biological consequences," *J. Am. Acad. Dermatol.* **58**(5 Suppl. 2), S139–S148 (2008).
34. J. Essers, W. Vermeulen, and A. B. Houtsmuller, "DNA damage repair: anytime, anywhere?" *Curr. Opin. Cell Biol.* **18**(3), 240–246 (2006).
35. R. B. Setlow, "The wavelengths in sunlight effective in producing skin cancer: a theoretical analysis," *Proc. Natl. Acad. Sci. U.S.A.* **71**(9), 3363–3366 (1974).
36. R. P. Sinha and D.-P. Häder, "UV-induced DNA damage and repair: a review," *Photochem. Photobiol. Sci.* **1**(4), 225–236 (2002).
37. C. Kielbassa, L. Roza, and B. Epe, "Wavelength dependence of oxidative DNA damage induced by UV and visible light," *Carcinogenesis* **18**(4), 811–816 (1997).
38. S. Mouret et al., "Cyclobutane pyrimidine dimers are predominant DNA lesions in whole human skin exposed to UVA radiation," *Proc. Natl. Acad. Sci. U.S.A.* **103**(37), 13765–13770 (2006).
39. S. Kozmin et al., "UVA radiation is highly mutagenic in cells that are unable to repair 7,8-dihydro-8-oxoguanine in *Saccharomyces cerevisiae*," *Proc. Natl. Acad. Sci. U.S.A.* **102**(38), 13538–13543 (2005).
40. A. J. Ridley et al., "Cellular and sub-cellular responses to UVA in relation to carcinogenesis," *Int. J. Radiat. Biol.* **85**(3), 177–185 (2009).
41. T. Douki et al., "Bipyrimidine photoproducts rather than oxidative lesions are the main type of DNA damage involved in the genotoxic effect of solar UVA radiation," *Biochemistry (N.Y.)* **42**(30), 9221–9226 (2003).
42. K. Ito, Y. Hiraku, and S. Kawanishi, "Photosensitized DNA damage induced by NADH: site specificity and mechanism," *Free Radic. Res.* **41**(4), 461–468 (2007).
43. Y. Jiang et al., "UVA generates pyrimidine dimers in DNA directly," *Biophys. J.* **96**(3), 1151–1158 (2009).
44. S. Mouret et al., "UVA-induced cyclobutane pyrimidine dimers in DNA: a direct photochemical mechanism?" *Org. Biomolec. Chem.* **8**(7), 1706–1711 (2010).
45. T. J. McMillan et al., "Cellular effects of long wavelength UV light (UVA) in mammalian cells," *J. Pharm. Pharmacol.* **60**(8), 969–976 (2008).
46. W. Denk, J. H. Strickler, and W. W. Webb, "Two-photon laser scanning fluorescence microscopy," *Science* **248**(4951), 73–76 (1990).
47. K. König et al., "Pulse-length dependence of cellular response to intense near-infrared laser pulses in multiphoton microscopes," *Opt. Lett.* **24**(2), 113–115 (1999).
48. P. Xi et al., "Two-photon imaging using adaptive phase compensated ultrashort laser pulses," *J. Biomed. Opt.* **14**(1), 014002 (2009).
49. P. Theer and W. Denk, "On the fundamental imaging-depth limit in two-photon microscopy," *J. Opt. Soc. Am. A* **23**(12), 3139–3149 (2006).